

Corrections to the generalized vector dominance due to diffractive ρ_3 production

I.P. Ivanov^{1,2*}, S. Pacetti³

¹ Fundamental Interactions in Physics and Astrophysics Group, Université de Liège, Belgium

² Sobolev Institute of Mathematics, Novosibirsk, Russia

³ LNF INFN, Frascati, Italy

Abstract

The idea of the vector dominance is still in use in various analyses of experimental data of photon-hadron reactions. It makes sense, therefore, to recast results of microscopic calculations of such reactions in this language. Here we present the diffractive DIS ρ_3 production as a specific correction to the generalized vector dominance. We perform a coupled channel analysis of spin-orbital excitations in diffractive photoproduction and reiterate the point that ρ_3 in diffractive DIS will be sensitive to a novel aspect of diffraction.

1 Introduction

The study of photon-hadron collisions in 1960's was driven to large extent by the Vector Dominance Model (VDM), the idea that the photon in such reactions behaves as a universal combination of hadrons with the photon's quantum numbers, see review [1]. In its simplest form, one assumes that the "hadronic part" of a physical photon in a given isospin-flavor channel is saturated by the ground state vector meson V contribution. If accompanied with the assumption that the subsequent interaction of this meson is a one-channel process, it yields direct relations among the cross sections of different processes, such as $\sigma(\gamma p \rightarrow Vp)$, $\sigma_{tot}(Vp)$, and $\sigma_{tot}(\gamma p)$ as well as decay width $\Gamma(V \rightarrow e^+e^-)$. Lifting some of these restrictions has lead to Generalized Vector Dominance (GVD) models, which provided rather good overall description of the data on the medium energy photon-hadron interactions.

The advent of partonic description of high-energy reactions as well as a vast amount of new data has set boundaries of the applicability of VDM/GVD. A particularly transparent insight into the nature of vector dominance is offered by the color dipole approach [2] (see next Section). Still, the physically appealing idea behind the vector dominance makes it an interesting exercise to recast results of a microscopic theory in a VDM-like form. An example of such analysis was given in Ref. [3] where the photoproduction of the radially excited meson $\rho(2S)$ off nuclei was found to be due to the off-diagonal transitions among different radial

*E-Mail: Igor.Ivanov@ulg.ac.be

excitations in diffraction. In a more recent example, [4, 5], the GVD was used to study the nature of a narrow dip structure in the 6π final state located near $M_{6\pi} \sim 1.9$ GeV.

In this paper we discuss the recent results on diffractive ρ_3 production [6], obtained within the k_t -factorization approach, in the GVD language. The $\rho_3(1690)$ meson cannot couple directly to the photon and therefore it is absent in the annihilation $e^+e^- \rightarrow \gamma^* \rightarrow \text{hadrons}$. But it can be produced diffractively, since diffraction conserves only the P - and C -parities but not the projectile spin J . Thus, ρ_3 production can be interpreted as a specific correction to the vector dominance model. With the coupled channel analysis we show that diffractive production of the D -wave spin-1 and spin-3 mesons of the ρ system, despite having comparable cross sections, probe very different aspects of diffraction.

The paper is organized as follows. In Section 2 we discuss relation between the (generalized) vector dominance models and the partonic description of diffraction. In Section 3 we argue that the diffraction operator does not conserve the spin of the projectile nor the angular momentum of the $q\bar{q}$ state, which represents the projectile in the first approximation. Production of ρ_3 , thus, can be viewed as a result of the off-diagonal transitions between different hadronic states in diffraction. In Section 4 we note that such a correction to VDM might have already been observed by the E687 experimentally. Possible nuclear effects and additional “photophobic” states are discussed in Section 5. Finally, in Section 6 we draw our conclusions.

2 (Generalized) Vector Dominance and its limits

Let us first remind the standard assumptions behind VDM and discuss the presence of excited mesons in the photon in this context.

In the original formulation, the physical photon is represented as a sum of a bare photon and of a “hadronic” part of the photon. Such decomposition is not Lorentz-invariant by itself, because what appears as a hadronic part of the photon in one frame of reference turns into a hadronic fluctuation of a target in another. One usually chooses the target rest frame, and if the photon energy is large enough, this decomposition is well defined. It is the hadronic part of the photon that participate in hadronic processes, while the bare photon contributes negligibly.

The hadronic part of the physical photon is represented as an integral over all possible *asymptotic* (in respect to strong interactions) hadronic states with photon’s quantum numbers and with invariant mass M . At not too large masses, the dispersion integral over M is saturated by the lowest resonances. Such contributions can then be *defined* as contributions of vector mesons. Limiting ourselves to the flavor-isospin sector that corresponds to the ρ mesons, one can rewrite the hadronic part of the (virtual) photon as

$$|\gamma^*(Q^2)\rangle_h = \sum_V \frac{e}{f_V} \frac{m_V^2}{m_V^2 + Q^2} |V\rangle. \quad (1)$$

The simplest VDM consists in assumption that only the ground state meson dominates in (1), which leads to

$$|\gamma^*\rangle_h = \frac{e}{f_\rho} \frac{m_\rho^2}{m_\rho^2 + Q^2} |\rho\rangle.$$

This assumption is often accompanied with an additional requirement that subsequent scattering process is *diagonal* in the space of states $|V\rangle$ in (1), and it then leads to direct relations

among various cross sections.

The presence of excited vector mesons in diffractive photoproduction calls to lifting the above restrictions. In the Generalized Vector Dominance (GVD) model one accepts (1) as it is, and assumes further that the subsequent interaction can lead to off-diagonal transitions among vector mesons $V_i \rightarrow V_f$.

2.1 GVD in the color dipole language

The origin of VDM/GVD success becomes transparent in the color dipole approach. It applies to the frame where projectile momentum is large, so that the transverse motion of partons is slowed down relativistically, and the fact that individual partons are not asymptotic states becomes inessential. In a high-energy diffractive reaction, the scattering amplitude has form $\mathcal{A}(A \rightarrow B) = \langle B | \hat{\sigma} | A \rangle$, where diffractive states are represented as coherent combinations of multipartonic Fock states:

$$|A\rangle = \Psi_{q\bar{q}}^A |q\bar{q}\rangle + \Psi_{q\bar{q}g}^A |q\bar{q}g\rangle + \dots \quad (2)$$

Here integration over all internal degrees of freedom assumed, and $\hat{\sigma}$ is the diffraction operator than describes the *diagonal* scattering of these multiparton states in the impact parameter representation. Switching from the basis of multipartonic states to the basis of physical mesons $\{|V_i\rangle\}$ and assuming completeness, one can recover (1).

Due to the lowest Fock state domination, the diffraction operator is based on the color dipole cross section $\sigma_{dip}(\vec{r})$ of a $q\bar{q}$ pair with transverse separation \vec{r} . The transition amplitude is represented as

$$\mathcal{A}(A \rightarrow B) = \int dz d^2\vec{r} \Psi_{q\bar{q}}^{B*}(z, \vec{r}) \sigma_{dip}(\vec{r}) \Psi_{q\bar{q}}^A(z, \vec{r}), \quad (3)$$

where z is the quark's fraction of the lightcone momentum of particle A .

The origin of the VDM success in reactions where A is the hadronic part of the photon lies in the fact that the typical wave functions of the ground state vector meson used in phenomenology are very similar to the transverse photon lightcone wave function at small Q^2 .

As virtuality Q^2 grows, the $q\bar{q}$ wave function of the photon shrinks, while the color dipole cross section behaves as $\sigma_{dip} \propto r^2$ at small r and reaches a plateau at large r . As a result, the function under integral (3), where $A \equiv \gamma^*$ and B is a ground state vector meson, peaks at the scanning radius $r_S \sim 6/\sqrt{Q^2 + M^2}$, see Ref. [7]. At small Q^2 the typical scanning radius is large, and the amplitude is roughly proportional to the integration measure

$$\mathcal{A}(\gamma^* \rightarrow V) \propto r_S^2 \propto \frac{1}{Q^2 + M^2},$$

which mimics the VDM behavior. At larger Q^2 the scanning radius becomes small enough and the diffraction cross section itself *decreases*. This phenomenon of color transparency produces a more rapid decrease $A(\gamma^* \rightarrow V) \propto 1/(Q^2 + M^2)^2$ up to logarithmic factors, [2, 7].

2.2 Presence of excited vector mesons in the photon

The behavior just described can be cast in the GVD language involving radial excitations [3]. At large Q^2 , the (small) photon must be represented as a coherent combination of a large

number of (big) radially excited states. Representing the diffractive production amplitude of a final meson V as

$$A(\gamma^*(Q^2) \rightarrow V) = \sum c_i(Q^2) \frac{M_i^2}{Q^2 + M_i^2} A(V_i \rightarrow V),$$

one sees that each term in this expansion decreases with Q^2 growth as $\propto 1/(Q^2 + M_i^2)$. However, coefficients $c_i(Q^2)$ must behave in such a way that cancellations among the terms makes the overall Q^2 -dependence of $A(\gamma^* \rightarrow V)$ is $\propto 1/(Q^2 + M_i^2)^2$, in accordance with color dipole result.

Note that similar arguments must be at work for the large- M photoproduction, when one studies the large-mass tail of broad resonances in a given (for example, multipion) final state. Production of a multipion state with invariant mass $M_{n\pi}$ significantly larger than the nominal mass of the vector meson must involve $q\bar{q}$ pairs with larger invariant mass, and smaller transverse separation, than for the vector meson at peak. In the color dipole approach this effect can be roughly accounted for by an additional correction factor

$$F(M_{n\pi}) = \frac{\sigma_{dip}(r_S(M_{n\pi}))}{\sigma_{dip}(r_S(M_V))} \quad (4)$$

in the amplitude. In the VDM language the same correction must be implemented as an additional $M_{n\pi}$ -dependence of the $\sigma(Vp \rightarrow Vp)$.

Another correction to VDM is related to the spinorial structure of the hadron's coupling to the $q\bar{q}$ state, implicitly present in (2) in the definition of $\Psi_{q\bar{q}}^A$. According to QED, the photon couples to the $q\bar{q}$ pair as $\bar{u}\gamma^\mu u$, but the corresponding coupling of a vector meson depends on $q\bar{q}$ angular momentum inside the meson. For the pure S -wave and pure D -wave vector mesons the structures $\bar{u}\Gamma^\mu u$ are [8]:

$$\Gamma_S^\mu = \gamma^\mu + \frac{2p^\mu}{M + 2m}, \quad \Gamma_D^\mu = \gamma^\mu - \frac{4(M + m)p^\mu}{M^2 - 4m^2}. \quad (5)$$

Thus, the photon coupling represents a specific form of S -wave/ D -wave mixing:

$$\gamma^\mu \Psi(q\bar{q}) = \Gamma_S^\mu \Psi_S(q\bar{q}) + \Gamma_D^\mu \Psi_D(q\bar{q}), \quad (6)$$

with appropriately normalized $\Psi_S(q\bar{q})$ and $\Psi_D(q\bar{q})$. Since the D -wave vector meson can be approximated by the $q\bar{q}$ pair in the $L = 2$ state, this proves that decomposition (1) must include orbitally excited vector mesons as well. The partial width $\Gamma(\rho'' \rightarrow e^+e^-)$ is known very poorly, [9], which gives us only very rough estimate $1/f_{\rho''} \sim 0.2(1/f_\rho)$, which gives a 20% contribution of the D -wave meson in (1). This value, however, supports the argument that the origin of D -wave state here is the quarks' Fermi motion.

There are two competing mechanisms for diffractive production of the orbitally excited vector mesons. First, the D -wave component of the photon in (6) can get "actuated" via diagonal scattering off the target. The other mechanism involves off-diagonal transition of the S -wave part of (6) into the D -wave vector meson under the action of diffraction operator. The k_t -factorization analysis of [10] did not specify which mechanism was the dominant. The coupled channel analysis presented in the following Section will help find the answer.

The same off-diagonal transitions that break the $q\bar{q}$ angular momentum conservation and produce a D -wave vector meson can also produce its spin-orbital partner, the D -wave spin-3

meson. Analysis of [6] in the case of $\rho_3(1690)$ showed that its production rate is expected to be only $2 \div 3$ times smaller than production rate of $\rho''(1700)$, which is believed to be predominantly D -wave vector meson. The hadronic part of the photon does not include the spin-3 meson, so it arises exclusively due to the off-diagonal properties of the diffraction operator.

3 Coupled channel analysis of the orbital excitations in diffraction

To get the GVD-like interpretation of the $\rho''(1700)$ and $\rho_3(1690)$ production, we perform a coupled channel analysis of the action of diffraction operator in the Fock subspace generated by three states in the ρ system: the ground state meson $\rho(770)$, which we identify with the pure $1S$ state, the excited vector meson $\rho''(1700)$, which we identify with a purely orbital excitation with $L = 2$, and the spin-3 meson $\rho_3(1690)$, which is also assumed to be in the $L = 2$ state.

3.1 Details of the numerical calculations

For numerical calculation of the diffractive transitions among these states, we use the k_t -factorization representation of the production amplitude. A generic amplitude of diffractive transition of an initial meson with polarization λ_i into the final meson with polarization λ_f is written within the k_t -factorization approach as

$$\frac{1}{s} \text{Im } A_{\lambda_f \lambda_i} = \frac{c_V \sqrt{4\pi \alpha_{em}}}{4\pi^2} \int \frac{dz d^2 \vec{k}}{z^2 (1-z)^2} \int \frac{d^2 \vec{\kappa}}{\vec{\kappa}^4} \alpha_s \mathcal{F}(x_1, x_2, \vec{\kappa}, \vec{\Delta}) \cdot \sum_{\text{diagr.}} I_{\lambda_f; \lambda_i} \Psi_f^*(\mathbf{p}_2^2) \Psi_i(\mathbf{p}_1^2). \quad (7)$$

Here z is the lightcone momentum fraction of the photon carried by the quark, \vec{k} is the relative transverse momentum of the $q\bar{q}$ pair, while $\vec{\kappa}$ is the transverse momentum of the gluon. Coefficient c_V is the standard flavor-dependent average charge of the quark, the argument of the strong coupling constant α_s is $\max[z(1-z)(Q^2 + M_i^2), \vec{\kappa}^2]$. The sum here runs over four standard diagrams with the two uppermost gluon legs attached to the $q\bar{q}$ dipole in all possible combinations.

Since to the leading $\log-1/x$ approximation the color dipole approach and the k_t -factorization approach are related by the transverse Fourier transform, the color dipole cross section is encoded within the k_t -factorization approach in the unintegrated gluon distribution. In our calculations, we used the fits to the unintegrated gluon distribution that were obtained in [11] by comparing the k_t -factorization calculations to the HERA F_{2p} data. In the present case, however, we need skewed unintegrated gluon distribution $\mathcal{F}(x_1, x_2, \vec{\kappa}, \vec{\Delta})$, where the fractions of the proton's momentum carried by the uppermost gluons are not equal, $x_1 \neq x_2$. To construct them, we use the simplified version of the well-known correcting factor [12] by simply rescaling the gluon momentum fraction by a universal factor 0.41, see details in [13].

The wave functions of the initial and final mesons were separated into the radial and angular parts, as described in [8]. The radial wave functions depend on

$$\mathbf{p}_i^2 = \frac{1}{4}(M_i^2 - 4m_q^2) = \frac{1}{4}M_i^2(2z - 1)^2 + \vec{k}_i^2 = k_{iz}^2 + \vec{k}_i^2, \quad i = 1, 2, \quad (8)$$

where M_i is the invariant mass of the initial ($i = 1$) and final ($i = 2$) $q\bar{q}$ pair. The integration variable \vec{k} is taken equal to the final transverse momentum, $\vec{k} = \vec{k}_2$, while the initial relative $q\bar{q}$ momentum \vec{k}_1 changes from one diagram to another. Note that since we deal with L eigenstates, it is vital to our approach to separate the three-dimensional radial and the angular parts. An approach where \vec{k} and z dependence of the wave functions are parametrized independently would be inadequate in our case.

The radial wave functions for the mesons were parametrized in the same way as in [10] and [6]. We used three-dimensional Gaussian and Coulomb (suppressed by an additional $1/M$ factor) radial wave functions. They roughly represent the two “extreme ends” of the whole spectrum of possible choices: a typical compact and a typical broad wave functions. Each of the parametrization was properly normalized and had one free parameter, the typical radius. This free parameter was adjusted so that the calculation of the $\Gamma(V \rightarrow e^+e^-)$ decay width reproduces the known data.

Since there is no data on the decay width of $\rho_3(1690)$ to e^+e^- , we used for the ρ_3 the same shape of the radial wave function as for the $\rho''(1700)$, only up to a different normalization factor. Since these two mesons are essentially spin-orbital partners, we believe that this approximation is reasonable.

Note that the radial wave functions of the three mesons considered do not have nodes. Therefore transitions from these states to radially excited states (i.e. transitions away from this subspace) are weak and can be neglected.

The angular properties of the wave functions of vector mesons were expressed via the spinorial structures (5). The spinorial structures for spin-3 meson were derived in [6]. All of them are already incorporated in the corresponding integrands $I_{\lambda_f;\lambda_i}$ in (7). These integrands represent, essentially, the trace over the quark loop with the specific spinorial structure inserted for the initial and final mesons. They are listed in the Appendix.

3.2 Expected uncertainties of the numerical results

We have checked that several parametrizations of the unintegrated gluon densities derived in [11] lead to numerical results differing at the several per cent level. The uncertainties related to the procedure of linking the skewed distributions to the diagonal ones have also been found small. So, the gluon distributions do not represent a significant source of uncertainties in the numerical calculations.

The major uncertainties come from the parametrizations of the radial wave functions. This is not surprising as our calculations of the ground state vector meson production, [11], as well as orbitally [10] and spin-excited [6] states were found to be sensitive to the wave function Ansatz, especially in the small- Q^2 limit of light mesons. The wave functions for the D -wave vector meson and spin-3 meson receive further uncertainty due to very poorly known experimental value of $\Gamma(\rho''(1700) \rightarrow e^+e^-)$. In our calculations, we used values $\Gamma(\rho''(1700) \rightarrow e^+e^-) = 0.14 \div 0.7$ keV.

We expect the uncertainty of the numerical results for the diagonal transitions $Vp \rightarrow Vp$ to be no more than factor of 2, while the non-diagonal transitions might be more uncertain. Note also that the photoproduction reaction, $\gamma p \rightarrow Vp$, is expected to be more sensitive to the details of the wave function parametrizations than the corresponding diagonal process $Vp \rightarrow Vp$.

3.3 Results for the transition matrix

Here, we present cross sections $\sigma_{ji} \equiv \langle j|\hat{\sigma}|i\rangle$ of transitions of an initial state i with a given transverse polarization into final state j with various polarization states.

We start with the forward scattering, $d\sigma_{ji}/dt$ at $t = 0$. In this case the strict s -channel helicity conservation (SCHC) takes place, and we are interested in transitions among transversely polarized states of ρ , ρ_D and ρ_3 . The calculations give the following matrix

$$\frac{d\sigma_{ji}}{dt} \Big|_{t=0} = \begin{pmatrix} 250 & 1.5 & 0.3 \\ 1.5 & 460 & 1.3 \\ 0.3 & 1.3 & 270 \end{pmatrix} \text{ mb}\cdot\text{GeV}^{-2}. \quad (9)$$

The off-diagonal values are non-zero, but stay small, which means that both total spin J and the $q\bar{q}$ angular momentum L are conserved only approximately.

We checked that the numerical results do depend on the details of the wave function parametrizations as anticipated. The off-diagonal elements in (9) show only the order of magnitude of the effect; the error by a factor of 2–3 can be present. The accuracy for the diagonal elements is somewhat higher, roughly within $\sim 50\%$.

To obtain the integrated cross sections, we calculate $d\sigma_{ji}/dt$ at non-zero t and integrate it within the region $|t| < 1 \text{ GeV}^2$. On passing to the non-forward cross sections, we must include the helicity amplitudes transition that violate SCHC. Such transitions give marginal contributions to the L -conserving diagonal transitions, but they are expected to be more important in the off-diagonal cases. In particular, results of [6] suggest that the ρ_3 production at small Q^2 can be even *dominated* by the helicity violating transitions.

Strictly speaking, in the non-forward case the diffraction operator acts in the $3+3+7 = 13$ -dimensional space of all helicity states of these three mesons. To keep the presentation clear, we show below the sum of cross sections of transitions from a given transversely polarized initial state to a final state with *all* possible helicities, which will make the transition matrix non-symmetric. The result of numerical integration is:

$$\sigma_{ji} = \begin{pmatrix} 19 & 1 & 0.2 \\ 1 & 27 & 0.3 \\ 1.3 & 0.4 & 19 \end{pmatrix} \text{ mb}. \quad (10)$$

Calculation showed that the diagonal elements are mostly due to helicity conserving transitions, while the off-diagonal elements receive very large contributions from helicity violating transitions, in agreement with expectations. Note very large difference between $\sigma(\rho_S \rightarrow \rho_3)$ and $\sigma(\rho_3 \rightarrow \rho_S)$, which also confirms domination of helicity violating transitions in ρ_3 production.

3.4 Difference in diffractive ρ_D and ρ_3 production

In order to understand the differences between photoproduction of ρ_D and ρ_3 , consider the initial photon as a vector in the subspace we consider. According to the discussion in Sect. 2.2, it can be represented roughly as $|\gamma\rangle \sim |\rho_S\rangle + 0.2|\rho_D\rangle$. One sees that direct “materialization” of the D -wave component of the photon followed by its diagonal scattering has much larger amplitude than the L -changing transition from the S -wave component (0.2 · 27 vs. 1).

On the other hand, the ρ_3 must appear in diffraction via the off-diagonal L - and J -violating elements of the diffraction operator (10). Thus, in contrast to the ρ_D , the ρ_3 production probes a *novel aspect of diffraction*.

4 Comparison between the 4π BaBar ISR and E687 data

In this section we discuss if the corrections to the GVD due to ρ_3 might have been already observed in experiment.

The dominant decay channel of ρ_3 is 4π with branching ratio $BR(\rho_3 \rightarrow 4\pi) = 73\%$. Thus one can look for its presence in diffractive photoproduction by comparing the rescaled E687 data [14] with BaBar initial state radiation (ISR) data [15] in $2(\pi^+\pi^-)$ final state.

Using GVD accompanied with the assumption that the diffraction operator is diagonal, one obtains the following relation between the 4π spectra in the e^+e^- annihilation and photoproduction:

$$\frac{1}{M_{4\pi}^2} \frac{d\sigma(\gamma p \rightarrow 4\pi p)}{dM_{4\pi}} \propto \sigma(e^+e^- \rightarrow 4\pi). \quad (11)$$

The presence of ρ_3 in diffraction should manifest itself as a bump in the photoproduction spectrum around $M_{4\pi} \sim 1.7$ GeV. If the above ideas of the dominance of SCHC violation in ρ_3 are correct, one will see a larger bump at higher values of $|t|$.

In Fig. 1 we present the 4π spectrum in e^+e^- annihilation obtained by BaBar and the diffractive photoproduction cross section from E687 modified according to (11). The relative normalization of the two data sets is adjusted manually for a better comparison of the resonance peaks.

There are three regions where deviations are seen. At $M_{4\pi} \approx 1.5$ GeV the BaBar data are significantly higher and at $M_{4\pi} \sim 1.7 \div 1.8$ GeV are somewhat lower than the rescaled E687 data. At $M_{4\pi} > 2$ GeV the BaBar data again take over. This region (zoomed in at the right plot of Fig. 1) seems the most disturbing, not only because the ratio between the two data sets here is large, but also because it increases with the $M_{4\pi}$ rise.

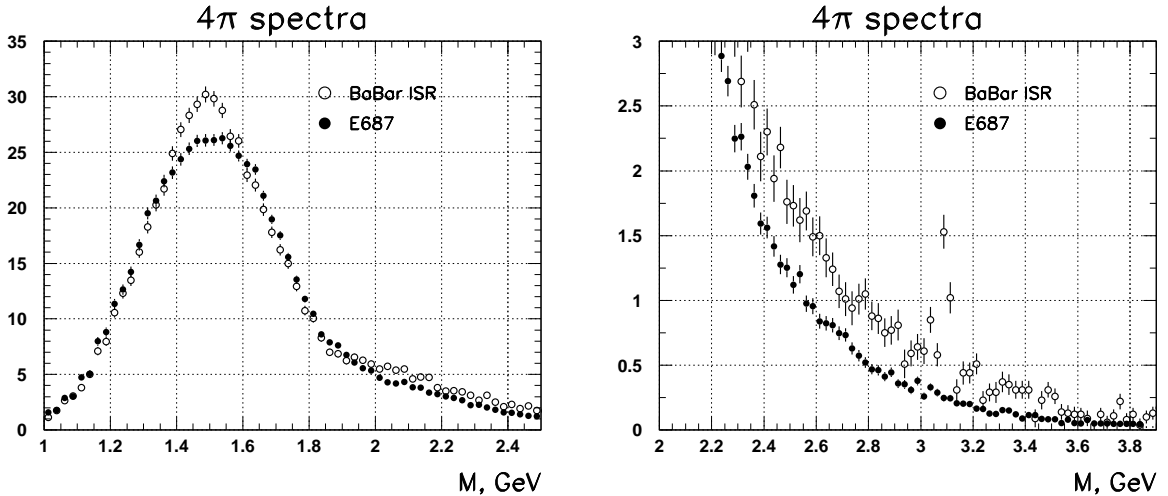


Figure 1: Comparison between the BaBar data and the E687 data weighted with $1/M_{4\pi}^2$ factor in the resonance region, left, and in the high mass region, right.

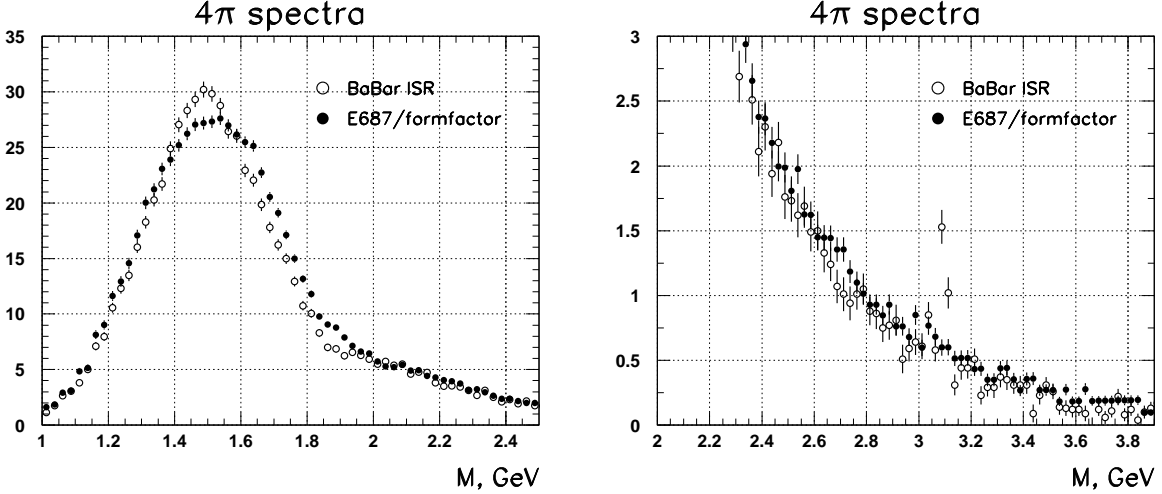


Figure 2: The same as in Fig. 1 but with the E687 data additionally corrected with the formfactor (12).

We argue that this high-mass discrepancy is an artefact of the naive VDM used in comparison (11). As discussed above, diffractive production of high mass multipion states are additionally suppressed in comparison with (11) by the factor (4). In a phenomenological analysis, this bias can be compensated by dividing the photoproduction data by the square of the correction factor (4). We used the well-known Golec-Biernat-Wüsthoff saturation model [16] for the color dipole cross section $\sigma(r) = \sigma_0[1 - \exp(-r^2/R^2(x))]$ and divided E687 data by the additional compensation factor

$$F(M_{4\pi}) = \left(1 - \exp\left[-\frac{10 \text{ GeV}^2}{M_{4\pi}^2}\right]\right)^2, \quad (12)$$

and then readjusted the overall normalization.

Figure 2 shows the results. The simple factor (12) makes the two data sets nearly identical in the entire high-mass range shown, $M_{4\pi} = 2.0\text{--}3.9$ GeV. In the resonance region, the balance between the two experiments changes. One sees a more prominent domination of the E687 data over the BaBar data in the range of $M_{4\pi} \sim 1.6 \div 1.9$ GeV, while the difference around $M_{4\pi} \approx 1.5$ GeV becomes less pronounced.

With these data sets only, one cannot draw a definitive conclusion about the origin of the broad 1.6–1.9 GeV peak seen in the *difference* of the data sets. It can be due to enhanced production of $\rho''(1700)$ or due to the presence of ρ_3 in photoproduction. If one assumes that it is *entirely* due to the presence of ρ_3 , one can roughly estimate its production rate,

$$\sigma(\rho_3)/\sigma(\rho' + \rho'') \sim 0.05 \div 0.1. \quad (13)$$

This number appears to be in agreement both with the old OMEGA result [17] and with calculations of [6]. We do not plunge here into a detail systematic analysis of the difference of the two data sets, but just state that it is worth studying further.

The easiest way to resolve the ambiguity in the origin of the enhancement would be to measure the same photoproduction spectrum at larger values of $|t|$ up to 1 GeV². If ρ_3 photoproduction is indeed dominated by the helicity-flip amplitudes, as argued in [6], its contribution should rapidly grow with $|t|$.

5 Discussion

5.1 Nuclear effects

A place where corrections to the naive VDM come to the foreground is diffractive production of excited mesons off nuclei. In this case the diffractive system can experience multiple scattering off separate nucleons, which amounts to multiple action of the diffraction operator on the initial state. Such action enhances the rate of production of excited states that were initially (almost) orthogonal to the photon. The fingerprints of this effect in experiment would be an observation of an A -dependence of the relative production rate of excited states, the modifications of the shape of these resonances and, possibly, novel interference patterns inside the nucleus.

Such in-medium modifications of the properties of the radially excited ρ states were explored in [3]. Even at moderate energies the shape of the $\rho(2S)$ state was noticeably distorted in heavy nuclei. The origin of this effect was traced back to non-trivial interplay between two production mechanisms: direct production $\gamma \rightarrow \rho(2S)$ and sequential transition $\gamma \rightarrow \rho(1S) \rightarrow \rho(2S)$. The latter transition is precisely due to the off-diagonal matrix element of the diffraction operator.

Similar effects are expected to take place in the orbitally excited sector of the diffractive states. In order to observe better the ρ_3 , one must focus not at the forward production, but at the entire region $|t| \lesssim 1 \text{ GeV}^2$. As was discussed above, the ρ_3 production is exclusively due to the off-diagonal matrix elements of the diffraction operator. Besides, according to (10), transitions from ρ_3 back to the ρ_S are less probable than the $\rho_S \rightarrow \rho_3$ transitions. All this produces a persistent "flux" towards the ρ_3 state, and its presence is enhanced upon each successive rescattering.

Note in addition, that production of ρ_3 in a given helicity state can proceed via many different helicity sequences, such as $\rho_S(\lambda_S) \rightarrow \rho_3(\lambda'_3) \rightarrow \rho_3(\lambda_3)$. All of them will interfere and might produce nontrivial patterns.

5.2 Photophobic states in diffraction

The ρ_3 is a state whose direct coupling to the photon is zero ("photophobic" state), yet it appears among diffractive states due to the off-diagonal transition. Similarly, one might expect that other hadrons not coupled directly to the photon might show up in diffraction. One interesting example is a hybrid meson. Phenomenologically, one often treats the hybrid (vector) meson as a state that does not couple directly to the photon, but it can reappear in photon's Fock state decomposition via hadronic loops and intermediate transitions to the nonexotic mesons. An analysis of this type was performed in [4, 5]. There, such a cryptoexotic state was assumed to couple to $\rho''(1700)$ but not to the photon. This simple model was proposed to explain the narrow dip structure in the 6π final state around $M_{6\pi} = 1.9 \text{ GeV}$ observed both in diffractive photoproduction [18] and in e^+e^- annihilation [15].

The present coupled channel analysis seems to be a more adequate framework for the analysis of possible interference effects of such photophobic states in diffraction. What one needs in order to get concrete predictions is a (phenomenological) microscopic model for such a state. Such an analysis would be complementary to that of [4, 5], since in these works the diffraction operator was assumed to be diagonal, while we show that this assumption is unwarranted. It would be interesting to see how non-diagonal transitions of the diffraction

operator influence the results of [4, 5].

6 Conclusions

Since the vector dominance idea is still used these days to understand some features of new experimental results, it is useful to discuss the results of microscopic QCD calculations in the language of the generalized vector dominance models. In this paper, we argued that the vector dominance model, when applied to the region $M \sim 1.5 - 2.0$ GeV, must receive significant corrections due to presence of the ρ_3 among diffractive states.

We compared the paths that lead to diffractive production of $\rho''(1700)$, which is believed to be a D -wave vector meson, and of $\rho_3(1690)$, its spin-orbital partner. Recent k_t -factorization results [6] show that their cross sections should be comparable. However, the coupled channel analysis performed here gives strong evidence that these two processes probe very different aspects of the diffraction. The $\rho''(1700)$ production can be viewed primarily as “materialization” of the D -wave component of the photon followed by diagonal diffractive scattering, while the ρ_3 production probes exclusively the off-diagonal elements of the diffraction operator. Thus, with ρ_3 one can study novel aspects of diffraction.

We also compared recent E687 and ISR BaBar data on 4π spectra obtained in diffraction and e^+e^- annihilation, respectively, and observed an enhancement in the photoproduction precisely where ρ_3 resides. At present it is not known if this enhancement is due to excited vector mesons or to the ρ_3 , but studies at non-zero momentum transfer t might provide the answer.

Finally, we discussed the role of orbital excitations in photon-nuclear collisions, and argued that the coupled channel analysis might help study other “photophobic” states.

Acknowledgements. The work was supported by FNRS and partly by grants RFBR 05-02-16211 and NSh-5362.2006.2.

A Transition amplitudes

The integrands $I_{\lambda_f \lambda_i}$ that appear in Eq. (7) are essentially the traces over the quark loop with specific spinorial structures inserted for the given initial and final spin, angular momentum and polarization states. They can be calculated directly as traces or can be constructed more efficiently via the light-cone spinor technique, which exploits the fact that the numerator of all four quark propagators can be taken on-mass-shell, see [13, 19].

For the S -wave to S -wave transition the integrands have form:

$$\begin{aligned} I_{00}^{SS} &= \frac{1}{4} M_1 M_2 \left[A_1 A_2 + \frac{4(\vec{k}_1 \vec{k}_2)(2z-1)^2}{(M_1 + 2m_q)(M_2 + 2m_q)} \right], \\ I_{++}^{SS} &= (\vec{k}_1 \vec{k}_2) + m_q^2 \left[B_1 B_2 + \frac{4(\vec{k}_1 \vec{k}_2)(2z-1)^2}{(M_1 + 2m_q)(M_2 + 2m_q)} \right], \\ I_{0+}^{SS} &= \frac{1}{2}(2z-1) M_2 \left[k_{2+} \frac{2m_q}{M_2 + 2m_q} - k_{1+} \frac{2m_q}{M_1 + 2m_q} A_2 + k_{1+} \frac{4(\vec{k}_1 \vec{k}_2)}{(M_1 + 2m_q)(M_2 + 2m_q)} \right], \end{aligned} \quad (14)$$

$$\begin{aligned}
I_{+0}^{SS} &= \frac{1}{2}(2z-1)M_1 \left[k_{1+}^* \frac{2m_q}{M_1 + 2m_q} - k_{2+}^* \frac{2m_q}{M_2 + 2m_q} A_1 + k_{2+}^* \frac{4(\vec{k}_1 \vec{k}_2)}{(M_1 + 2m_q)(M_2 + 2m_q)} \right], \\
I_{-+}^{SS} &= k_{1+} k_{2+} \left[1 - \frac{4m_q^2(2z-1)^2}{(M_1 + 2m_q)(M_2 + 2m_q)} \right] - (k_{1+})^2 \frac{2m_q}{M_1 + 2m_q} B_2 - (k_{2+})^2 \frac{2m_q}{M_2 + 2m_q} B_1,
\end{aligned}$$

and the remaining integrands can be obtained by appropriate change of + to - together with factor $(-1)^{\lambda_i + \lambda_f}$. Here $k_{i\pm} = -(k_{i\mu} e^\mu_\pm) = -k_{i\mp}^*$, and

$$A_i = 4z(1-z) + \frac{2m_q}{M_i + 2m_q} (2z-1)^2, \quad B_i = 1 + \frac{\vec{k}_i^2}{m_q(M_i + 2m_q)}.$$

Corresponding expressions for all other possible transitions among S -wave, D -wave and spin-3 states can be obtained by the projection technique described in [8, 6]. For example, the corresponding integrands for the spin-3 meson transition from polarization state λ_i to λ_f can be described by 7×7 matrix:

$$I_{\lambda_f \lambda_i}^{33} = T_{\lambda_f \lambda'}^{3S} I_{\lambda' \lambda}^{SS} T_{\lambda \lambda_i}^{S3}, \quad (15)$$

where “transition matrices” can be readily constructed from the Clebsch-Gordan coefficients involved in description of the spin-3 meson, see Ref. [6]. For example,

$$T_{\lambda \lambda_i}^{S3} = \begin{pmatrix} k_+^2 & \frac{2}{\sqrt{3}} k_z k_+ & \frac{1}{\sqrt{15}} (2k_z^2 - \vec{k}^2) & \frac{2}{\sqrt{10}} k_z k_- & \frac{1}{\sqrt{15}} k_-^2 & 0 & 0 \\ 0 & \frac{1}{\sqrt{3}} k_+^2 & \frac{4}{\sqrt{15}} k_z k_+ & \frac{1}{\sqrt{10}} (2k_z^2 - \vec{k}^2) & \frac{4}{\sqrt{15}} k_z k_- & \frac{1}{\sqrt{3}} k_-^2 & 0 \\ 0 & 0 & \frac{1}{\sqrt{15}} k_+^2 & \frac{2}{\sqrt{10}} k_z k_+ & \frac{1}{\sqrt{15}} (2k_z^2 - \vec{k}^2) & \frac{2}{\sqrt{3}} k_z k_- & k_-^2 \end{pmatrix}, \quad (16)$$

where subscript 1 is assumed for all the momenta, while matrix T^{3S} is just the hermitian conjugate of T^{S3} with replacement $k_1 \rightarrow k_2$. Similar expressions can be obtained also for the D -wave vector mesons.

References

- [1] T. H. Bauer, R. D. Spital, D. R. Yennie and F. M. Pipkin, Rev. Mod. Phys. **50** (1978) 261 [Erratum-ibid. **51** (1979) 407].
- [2] N. N. Nikolaev and B. G. Zakharov, Z. Phys. C **49** (1991) 607; A. H. Mueller, Nucl. Phys. B **335** (1990) 115; N. N. Nikolaev, Comments Nucl. Part. Phys., **21** (1992) 41.
- [3] N. N. Nikolaev, J. Speth and B. G. Zakharov, Phys. Atom. Nucl. **63** (2000) 1463 [Yad. Fiz. **63** (2000) 1463].
- [4] P. L. Frabetti *et al.*, Phys. Lett. B **578** (2004) 290.
- [5] R. Baldini *et al.*, Eur. Phys. J. A **31** (2007) 645.
- [6] F. Caporale, I. P. Ivanov, Eur. Phys. J. C **44** (2005) 505.
- [7] B. Z. Kopeliovich, J. Nemchik, N. N. Nikolaev and B. G. Zakharov, Phys. Lett. B **309** (1993) 179; J. Nemchik, N. N. Nikolaev and B. G. Zakharov, Phys. Lett. B **341** (1994) 228.

- [8] I. P. Ivanov and N. N. Nikolaev, JETP Lett. **69** (1999) 294.
- [9] W.-M. Yao *et al.* [Particle Data Group], J. Phys. G **33** (2006) 1.
- [10] F. Caporale and I. P. Ivanov, Phys. Lett. B **622** (2005) 55.
- [11] I. P. Ivanov and N. N. Nikolaev, Phys. Rev. D **65** (2002) 054004.
- [12] A. G. Shuvaev, K. J. Golec-Biernat, A. D. Martin and M. G. Ryskin, Phys. Rev. D **60** (1999) 014015.
- [13] I. P. Ivanov, N. N. Nikolaev and A. A. Savin, Phys. Part. Nucl. **37** (2006) 1
- [14] P. Lebrun [E687 Collaboration], FERMILAB-CONF-97-387-E, *talk given at the 7th International Conference on Hadron Spectroscopy (Hadron 97), Upton, NY, 25-30 Aug 1997*.
- [15] B. Aubert *et al.* [BABAR Collaboration], Phys. Rev. D **71** (2005) 052001.
- [16] K. Golec-Biernat and M. Wusthoff, Phys. Rev. D **59** (1999) 014017.
- [17] M. Atkinson *et al.* [Omega Photon Collaboration], Z. Phys. C **30** (1986) 531.
- [18] P. L. Frabetti *et al.* [E687 Collaboration], Phys. Lett. B **514** (2001) 240.
- [19] I. P. Ivanov, PhD thesis, Bonn University, 2002, arXiv:hep-ph/0303053.